Hindawi
Geofluids
Volume 2021, Article ID 6658729, 15 pages
https://doi.org/10.1155/2021/6658729

Research Article

Impact of High Thermal Setting and Fluid Activities on Sandstone Compaction: A Case Study of the Baiyun Sag in the Pearl River Mouth Basin (Northern South China Sea)

Chi Li[1], **Jinglan Luo**[1], **Caiwei Fan**[2], **Shanshan Li**[2], **Shijiu Wu**[2], **Chuan Lei**[3] and **Kunpeng Song**[1]

[1]*State Key Laboratory of Continental Dynamics, Department of Geology, Northwest University, Xi'an 710069, China*
[2]*Zhanjiang Branch of CNOOC Ltd., Zhanjiang 524057, China*
[3]*Chang'an University, Xi'an 710021, China*

Correspondence should be addressed to Jinglan Luo; jlluo@nwu.edu.cn

Received 20 October 2020; Revised 15 February 2021; Accepted 20 February 2021; Published 15 March 2021

Academic Editor: Xiaorong Luo

Compaction is regarded as central to the reduction of reservoir physical properties. The thermal compaction process controlled by a basin's heat flow and the static compaction caused by overload on rocks are both important factors controlling the compaction strength. However, porosity loss resulting from thermal and static compaction has not been distinguished. The Baiyun Sag in the Pearl River Mouth Basin in the northern part of the South China Sea with high heat flows and a variable geothermal gradient is an ideal setting for studying the characteristics and mechanisms of the thermal compaction process. The characteristics of compaction and the effect of thermal fluid activities on reservoir physical properties are carried out, based on the observation and identification of sandstone thin sections under a microscope, the measurement and simulation of the temperatures and trapping pressures of fluid inclusions, and the calculation of the compaction porosity loss as well. The result shows that the compaction mode of sandstone reservoirs in the Zhuhai Formation is dominated by static compaction in the LGR (the low geothermal gradient region), whereas the diagenetic process of the Zhuhai Formation in the MGR (the moderate geothermal gradient region) and HGR (the high geothermal gradient region) is affected not only by the static compaction effect but also by the thermal compaction effect caused by abnormal formation temperature and pressure conditions. The porosity loss caused by the thermal compaction ranges from 5.5% to 11.2% with an average of 7.9% and from 4.6% to 16.6% with an average of 10.2% in the MGR and HGR, respectively. The porosity loss caused by the static compaction ranges from 15.9% to 20.8% with an average of 19.4% and from 8.4% to 15.8% with an average of 12.8% in the MGR and HGR, respectively.

1. Introduction

Compaction is an important component of diagenesis and is regarded as central to the reduction of reservoir physical properties [1–5]. In classical diagenetic theory, it is believed that the compaction of clastic sediments is caused by the effective stress of the overlying stratum [6]. The porosity and permeability of sediments decrease with the thickening of overlying strata, the deepening of deposited clastic sediments, and increasing temperature and pressure [5].

Recently, it was found that the compaction of reservoirs is controlled not only by the load of overlying rocks and types of sediments present but also by other factors such as properties of porosity fluids, the geothermal gradient of basins, and burial-thermal evolution routes [3, 7–9].

The thermal compaction process controlled by a basin's heat flow and the static compaction process caused by overloaded rocks are both important factors in controlling the compaction strength, and this diversity in the compaction mechanisms of clastic rocks is caused by complex geological conditions such as temperature-pressure fields [6, 10, 11]. It has been reported that porosity loss caused by thermal compaction is common in basins with high heat flow, demonstrating a tendency of increasing compaction strength with

increasing temperature and geothermal gradient (Gra) under the same sedimentary conditions [10, 12]. In addition, it has been indicated that an uprise of the geothermal gradient (Gra) can increase the rate of porosity loss in sandstones [13].

The present features of the formation are mainly attributed to the burial-diagenetic evolution history under the geological setting including the ancient and the present heat flow and geothermal gradient. The physical properties of sandstones gradually evolved into their current performance under the local physical and chemical conditions [12]. If the strata are affected by hydrothermal fluids, the temperature attained during the geological history can be different from the present temperature. Secondary fluid inclusions, formed during the diagenetic process and contained important information of the paleotemperature, paleopressure, and paleofluid compositions of reservoirs, can provide vital basis for the study of the source and migration of fluids and the diagenetic evolution process [14–17]. The homogenization temperature and trapping pressure of the secondary fluid inclusions in sandstones reflect the temperature and pressure of porosity fluids captured at the time, respectively. Therefore, a reservoir affected by thermal fluid activities can be traced from the trapping pressure and the homogenization temperature that is higher than that of the strata temperature reached under the normal geothermal gradient from fluid inclusions captured during the diagenetic process [17, 18] and from analysis of carbon, oxygen, and strontium isotopic of cements as well [19, 20].

The Baiyun Sag, in the Pearl River Mouth Basin in the northern South China Sea with high heat flows and variable geothermal gradients, is an ideal setting for studying the characteristics and mechanisms of the thermal compaction process. Previous researches have shown that high geothermal gradient accelerated the rate of clay mineral transformation and changed the precipitation-dissolution equilibrium state of carbonate cements, which in turn affects their vertical distribution. The disappearing buried depths of kaolinite and mixed layer of smectite/illite clay mineral in the high geothermal gradient area are shallower than those in the low geothermal gradient area [12, 21, 22]. The dissolution of carbonate cements is stronger in the high geothermal gradient area than that in the low geothermal gradient one [12, 21, 22]. The compaction process of sandstones in the "hot basin" of the Baiyun Sag is more complex. However, research on porosity loss caused by the thermal compaction process is still insufficient. Porosity loss caused by thermal and static compaction is not distinguished when the compaction mechanisms of sandstone reservoirs are discussed [10].

The characteristics of compaction and the influence of thermal fluid activities on reservoir physical properties are studied, based on sandstone samples from the Zhuhai Formation in the Baiyun Sag, and thermal compaction and its quantitative calculation methods for reservoir porosity loss are proposed. The presented results will be helpful in understanding the impact of high thermal setting and fluid activities on sandstone compaction and porosity loss, clarifying the diagenetic evolution model of sandstone reservoirs, and providing a reference for the prediction of favorable areas of reservoirs in basins with variable geothermal gradients.

2. Geological Setting

The Baiyun Sag, located in the deep-water area of the Pearl River Mouth Basin of the northern South China Sea, is a mega depression with an area of over 12,000 km^2 and a current water depth of 200 m to 3,000 m [23]. The Pearl River Mouth Basin has experienced three major tectonic evolution stages including extensional rifting stage, postrifting subsidence depression stage, and fault block lifting stage, since the Cenozoic, and was in an extension environment with multiperiod structural movements including the Zhuqiong movement, Nanhai movement, Baiyun movement, and Dongsha movement [24, 25]. Particularly, the Baiyun movement (23.8 Ma) accompanied by the transition of the spreading ridge during the Neogene, a rapid migration (23.8 Ma) of the shelf edge from the southern part to the northern part of the Baiyun Sag occurred, which resulted in strong accelerated subsidence and multistage magmatic activities in the Baiyun Sag [26–29].

Different from craton basins, the crust of the Baiyun Sag is thinner, its mantle-crust interface is shallower, and the heat flow is high due to the southward transition of the spreading ridge and intense thinning of the crust caused by the Baiyun movement [30, 31]. The heat flux from the deep mantle accounts for a higher percentage of the total heat flow, while the crustal heat flow contributes relatively a lower percentage [32, 33], which means the thinner the lithosphere, the more heat is transferred from the mantle in the Pearl River Mouth Basin [33]. It has been reported that the high heat flows found in the South China Sea. The Pearl River Mouth Basin, located in the northern part of the South China Sea, is a typical hot basin with heat flow values at present range from 24.2 mW/m^2 to 121.0 mW/m^2 with an average of 71.8 ± 13.6 mW/m^2 [34–37]. The present geothermal gradient (Gra) in the Baiyun Sag of the southern Pearl River Mouth Basin increases gradually from north to south (Figure 1), which is mainly attributed to magma and fault activities caused by crust thinning occurring in the Cenozoic [36], and due to Neotectonics since 13.8 Ma accompanied by active thermal fluid activities in the southern part of the Baiyun Sag, with the highest current geothermal gradient of 66.4°C/km in the south [33]. Previous research shows that the diagenetic process and reservoir quality evolution of sandstones in Baiyun Sag were affected by both the high thermal setting and thermal fluid activities, which enhanced the compaction and cementation, and accelerated the clay mineral transformation [21]; the high thermal setting and fluid activities are both critical factors on sandstone compaction and porosity loss.

3. Methodology

3.1. Observation and Identification of Thin Sections. A total of 141 sandstone core samples of the Oligocene Zhuhai Formation taken from 10 wells in the Baiyun Sag were examined in this study. Based on observation and identification of thin sections under a microscope, the percentage of each fragment, the matrix, and authigenic minerals was approximately estimated, and statistics of all kinds of pores and contact

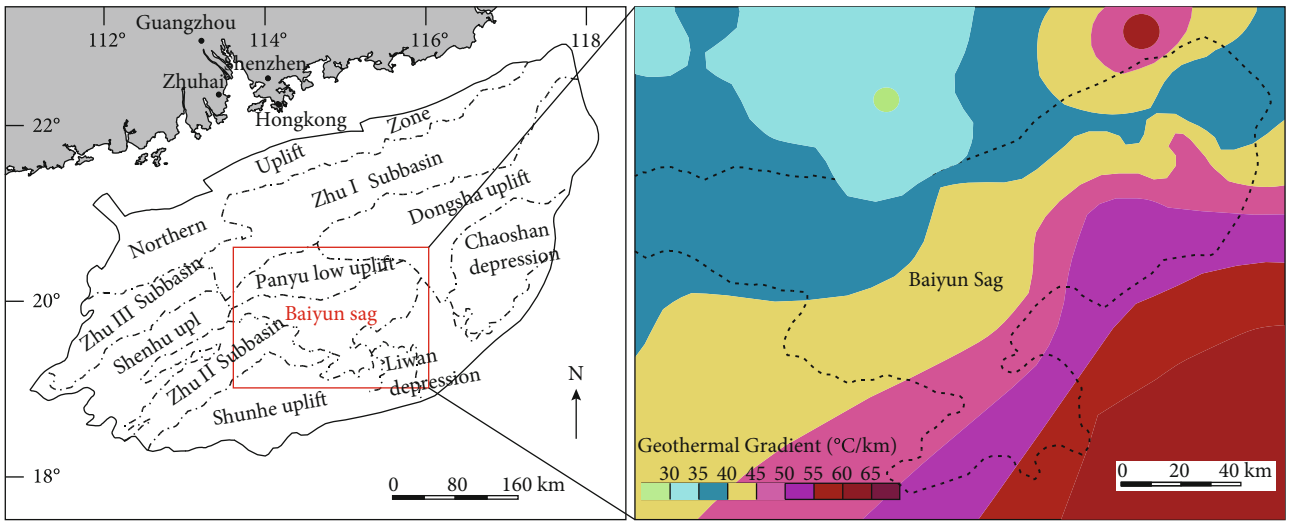

(a) (b)

Figure 1: Location and current geothermal gradient distribution of Baiyun Sag, Pearl River Mouth Basin: (a) location of the Pearl River Mouth Basin in China; (b) horizontal distribution of current geothermal gradient in Baiyun Sag.

patterns between detrital minerals have been made by the visual estimation method, using a set of standard mineral content patterns as our comparison criteria.

3.2. Porosity Loss Calculation. The porosity loss caused by compaction can be calculated using the following formulas.

The original porosity (OP, %) of the Zhuhai Formation sandstones can be recovered by the following empirical formula [38]:

$$\mathrm{OP} = 20.91 + \frac{22.9}{S_0}. \quad (1)$$

In formula (1), $S_0 = (P_{25}/P_{75})^{1/2}$; P_{25} and P_{75} represent the grain diameters corresponding to the content at 25% and 75%, respectively, on the grain size accumulation curve.

Assuming that the original volume of a rock decreases during compaction and that the intergranular volume (IGV) remains, the compaction porosity loss (COPL) of sandstone in the Zhuhai Formation can be calculated using the following formula [39]:

$$\mathrm{COPL} = \mathrm{OP} - \left[\mathrm{IGV} \times \frac{1 - \mathrm{OP}}{1 - \mathrm{IGV}}\right]. \quad (2)$$

This method assumes that compaction occurs prior to cementation and dissolution, so the intergranular volume (IGV) includes the pore volume filled by cementation that is intergranular pores, in addition to the volume of matrix and cements. The increased pore volume due to the dissolution of matrix should be removed, making the calculation of porosity loss accurate [4].

$$(\mathrm{IGV} = \text{intergranular pores} + \text{matrix} + \text{cements}). \quad (3)$$

The compaction rate (CR) can be calculated by the following formula:

$$\mathrm{CR} = \frac{\mathrm{COPL}}{\mathrm{OP}} \times 100\%. \quad (4)$$

3.3. Measurement of Temperature and Simulation of the Trapping Pressure of Fluid Inclusions. The homogenization temperature and freezing temperature of gas-liquid secondary brine inclusions (hydrocarbon-containing) found at the quartz overgrowths or in healed cracks in quartz of sandstones in the Zhuhai Formation were measured at a LINKAM THMS600 INSTEC, which was calibrated using synthetic pure-CO_2 fluid inclusions (melting point: -56.6°C), pure water (melting point: 0°C), naphthalene (melting point: 78.2°C), and adipic acid (melting point: 152.1°C). Test conditions are as follows: temperature 20°C, humidity 30%, and experiment error ±0.1°C. Fluid inclusions that showed obvious signs of necking down, leakage, or stretching were not measured by microthermometry.

The measurement of the inclusion homogenization temperature-salinity method was used to recover the trapping pressure of fluid inclusions and to represent the paleopressure of the formation during the fluid filling period, based on the measurement result of inclusion temperature. The salinity of the inclusion fluid was calculated by the salinity-freezing point formula of the H_2O-NaCl system [40]. The formula is as follows:

$$w = 1.78 \times Tm - 0.0442 \times Tm^2 + 0.000557 \times Tm^3. \quad (5)$$

In formula (5), w is the NaCl weight percentage (%), and Tm is the absolute value of the freezing temperature (°C).

It has been reported that there is a certain functional relationship between the homogenization temperature, salinity, and paleopressure of fluid inclusions, and the minimum

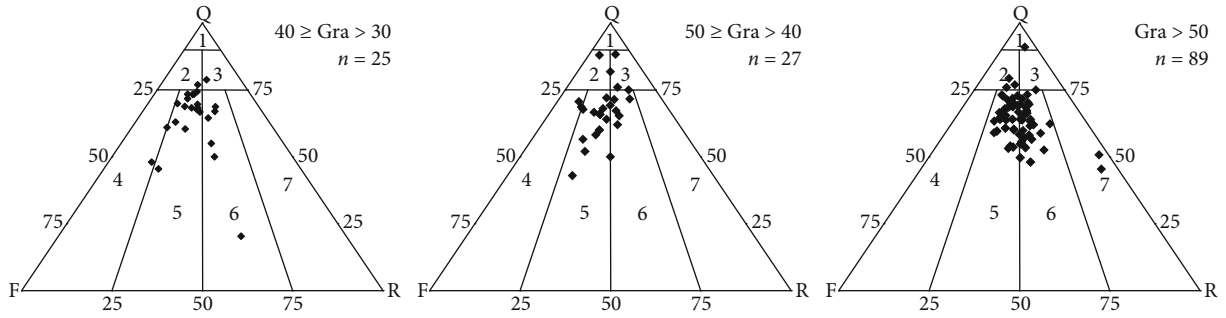

Figure 2: Sandstone classification of Zhuhai Formation in different geothermal gradient regions: (1) quartzarenite, (2) subarkose, (3) sublitharenite, (4) arkose, (5) lithic arkose, (6) feldspathic litharenite, and (7) litharenite.

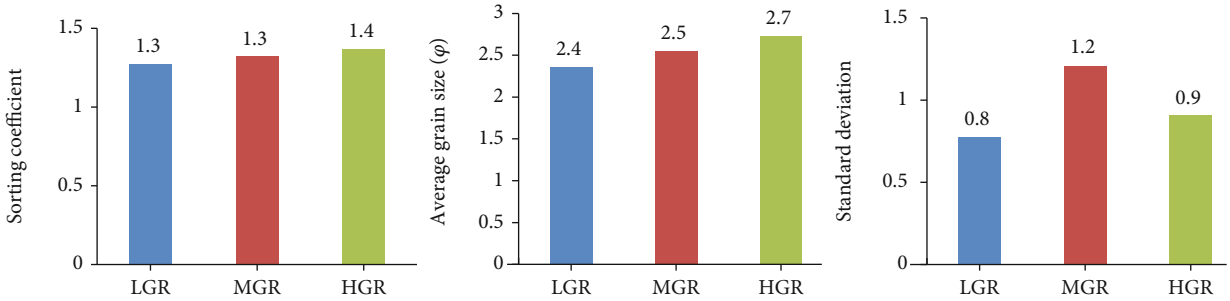

Figure 3: Sedimentary characteristics of sandstones in Zhuhai Formation in different geothermal gradient regions.

trapping pressure of fluid inclusions can be obtained by the following formulas [41]:

$$f = (A_1 + A_2 \times T) \times 10^{-1}, \tag{6}$$

$$\begin{aligned} A_1 = {} & 6.1 \times 10^{-3} + \left(2.383 \times 10^{-1} - a1\right) \\ & \times T_h - \left(2.855 \times 10^{-3} + a2\right) \\ & \times {T_h}^2 - \left(a_3 \times T_h + a_4 \times {T_h}^2\right) \\ & \times 1000 \times \frac{w}{[58.5 \times (100 - w)]}, \end{aligned} \tag{7}$$

$$\begin{aligned} A_2 = {} & a_1 + a_2 \times T_h + 9.888 \times 10^{-6} \\ & \times {T_h}^2 + (a_3 + a_4 \times T_h) \\ & \times 1000 \times \frac{w}{[58.5 \times (100 - w)]}. \end{aligned} \tag{8}$$

In (6), (7), and (8) formulas, f is the minimum trapping pressure (MPa); T is the trapping temperature (°C, 15°C higher than the homogenization temperature [42]); T_h is the homogenization temperature (°C); w is salinity (wt%); a_1, a_2, a_3, and a_4 are constants; and for the H_2O-NaCl system, $a_1 = 28.73$, $a_2 = -0.06477$, $a_3 = -0.2009$, and $a_4 = 0.003186$ [42].

Then, the paleopressure coefficient (λ) can be obtained from paleopressure data by using the following formula [42]:

$$\lambda = \frac{f}{fw} = \frac{f}{\rho \times g \times h/1000}. \tag{9}$$

In formula (9), f_w is ancient hydrostatic pressure (MPa); h is ancient burial depth (m); g is acceleration due to gravity (9.8 m/s^2); and ρ is the density of brine fluid (g/cm^3), which can be obtained from the formula for the fluid density of brine inclusion [43].

3.4. Thermal Region Division according to Different Geothermal Gradients. The geothermal gradient, also known as the "geothermal heating rate," refers to the growth rate of the formation temperature with an increase in burial depth without the influence of atmospheric temperature. Its regional variation may come from a change in the heat flow rate or from a change in the thermal conductivity of the near-surface rock body.

Research on the relationship between the geothermal gradient and sandstone porosity shows that the geothermal field clearly controls pore evolution and porosity change. For example, the buried depth of the stratum with a porosity of 10% to 15% can differ from 2.5 km to 3.0 km when the geothermal gradient rises from 20°C/km to 40°C/km, respectively. The porosity of sandstone decreases slowly with increasing burial depth in low geothermal gradient basins, where the effective reservoirs in deeper can be still found. However, in high geothermal field basins, the porosity of sandstone decreases rapidly with increasing burial depth, and the burial depths of effective reservoirs are shallower than that of in the low geothermal field basins [44].

The present geothermal gradients (Gra) in the Baiyun Sag gradually increase from north to south, and there is evidence that the diagenetic evolution of reservoirs is affected by deep thermal fluids [12, 21, 22, 45, 46]. To analyze the

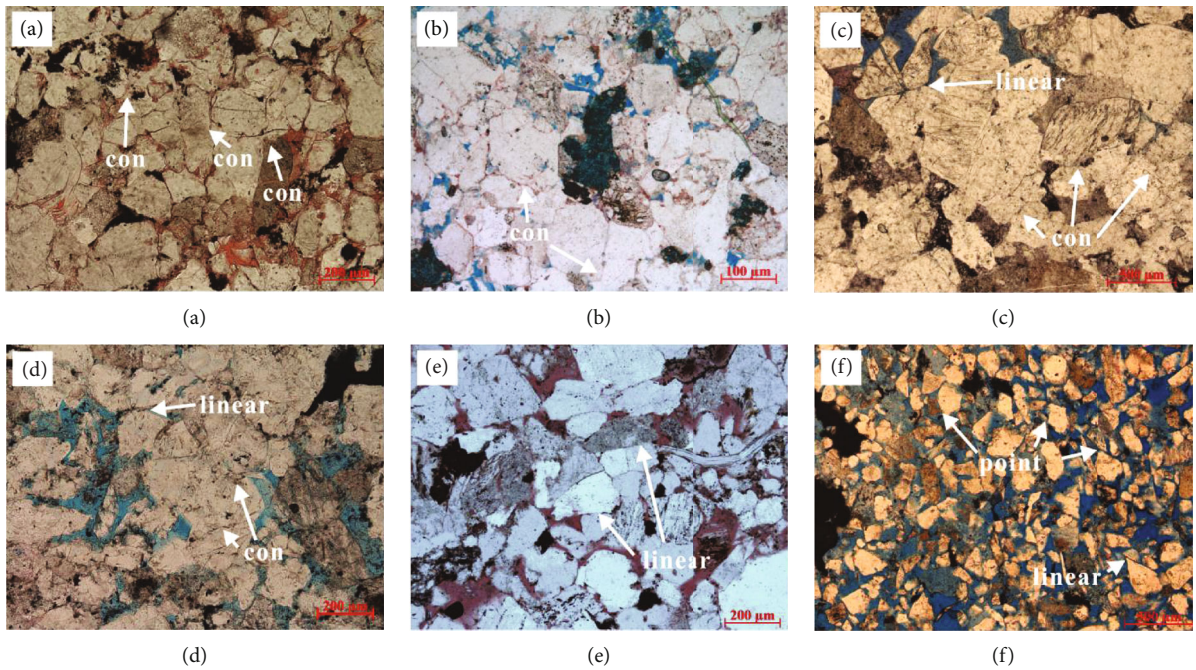

(a) (b) (c)

(d) (e) (f)

Figure 4: Microscopic characteristics of sandstone compaction in Zhuhai Formation: (a) contact between detrital minerals in sandstones is mainly concavo-convex (con), Y33-1, Gra = 35.6°C/km; (b) contact between detrital minerals in sandstones is mainly concavo-convex (con), Y35-2, Gra = 39.3°C/km; (c) contact between detrital minerals is mainly linear and concavo-convex (con), W3-2, Gra = 47.2°C/km; (d) contact between detrital minerals is mainly linear and concavo-convex (con), H34-6, Gra = 48.0°C/km; (e) contact between detrital minerals is mainly linear, W3-1, Gra = 53.0°C/km; (f) contact between detrital minerals is mainly point and linear, W21-1, Gra = 66.4°C/km.

Table 1: The original porosity (OP) and porosity loss by compaction (COPL) of sandstones in the Zhuhai Formation.

Region	Well	Gra at present (°C/km)	Burial depth (m)	OP (%)	COPL (%)	CR (%)
LGR	Y25-2	33.6	3374.1	38.7	29.1	75.0
	Y3-1	36.6	3689.1	38.9	34.2	88.0
	Y35-2	39.3	3849.9	39.0	30.2	77.6
MGR	H23-1	40.7	2348.8	39.1	28.4	72.6
	Y16-1	44.2	2399.7	38.8	27.3	70.2
	H16-2	45.5	1847.0	40.0	21.4	53.4
	W3-2	47.2	2413.9	37.6	32.0	85.2
HGR	W3-1	53.0	1829.5	38.5	25.3	65.9
	W3-13	55.9	1657.7	37.0	18.8	51.0
	W21-1	66.4	972.3	38.8	25.0	64.3

influence of thermal setting and fluid activities on the compaction effect, the study area was divided into three regions according to the present geothermal gradient: the low geothermal gradient region (LGR, Gra ≤ 40°C/km), the moderate geothermal gradient region (MGR, 50°C/km ≥ Gra > 40 °C/km), and the high geothermal gradient region (HGR, Gra > 50°C/km). The characteristics of and differences in the compaction effects in different regions were compared.

4. Results

4.1. Sandstone Petrography and Compaction Characteristics. Generally, the quality of a reservoir is determined not only by diagenesis but also by sedimentation. The compaction of sandstone is carried out by the subsidence of clastic particles, which reduces the distance between particles and decreases the volume of sediments, and it is also controlled by sedimentary conditions such as grain size, sorting, roundness, and detrital and matrix content. The plastic deformation of detrital grain and matrix under compaction can increase contact between grains and make sandstones more compact. Therefore, the mineral composition and grain size of sandstones from the high and low geothermal gradient areas were firstly compared in this study. Only on the premise that the sedimentary conditions are basically the same can we compare the differences in diagenesis and analyze the influence of diagenesis on reservoir quality.

The results of observations and quantitative statistics from thin sections under a microscope in the study area show that the rock types of the sandstones in the Zhuhai Formation are basically the same, mainly including medium- to fine-grained lithic arkose and feldspathic litharenite (Figure 2). The matrix content in sandstones is lower than 5%, and the average grain size and sorting coefficient of all

Table 2: Temperature, salinity, and trapping pressure of fluid inclusions of sandstones in the Zhuhai Formation.

Region	Well	Current Gra (°C/km)	Current pressure coefficient	Homogenization temperature (°C)			Freezing temperature (°C)			Salinity (wt%)			Ancient burial depth (m)	Trapping pressure (MPa)	Paleopressure coefficient
				Min.	Max.	Mean	Min.	Max.	Mean	Min.	Max.	Mean			
LGR	Y27-2	34.7	1.00	148.8	178.5	165.6	-16.7	-0.9	-8.1	1.6	19.9	11.0	4156.8	36.12	0.90
	Y20-1	35.4	1.17	108.0	163.0	134.5	-18.0	-0.4	-8.3	0.7	20.9	10.8	2657.2	38.66	1.47
	Y33-1	35.6	1.02	142.0	215.0	157.7	-15.0	-1.3	-6.0	1.7	18.6	4.2	3022.0	36.09	1.30
	Y35-25	38.5	1.08	152.8	188.2	172.5	-12.8	-3.1	-8.7	5.1	16.7	12.1	3188.0	35.78	1.16
	Y35-2	39.3	1.11	144.8	178.8	163.5	-8.7	-0.1	-3.5	0.2	12.5	5.4	3845.4	35.70	1.00
MGR	W3-2	47.2	1.07	100.0	151.0	128.5	-7.9	-0.3	-2.8	0.9	12.4	4.7	2073.7	38.57	1.96
	H34-6	48.0	1.03	96.7	236.6	146.1	-10.2	-0.3	-5.1	0.5	14.1	7.9	2192.6	37.51	1.79
HGR	H21-1	51.0	1.08	113.0	124.0	118.3	-9.6	-0.1	-1.7	1.4	6.6	3.0	2317.8	39.41	1.79
	W9-1	52.1	1.06	102.3	124.6	113.1	-11.1	-0.4	-4.8	0.7	15.1	7.4	1594.1	40.10	2.57
	W3-1	53.0	1.07	87.9	178.7	111.6	-17.4	-0.1	-4.4	0.2	20.5	3.7	1721.6	40.09	2.45

samples show few differences (Figure 3). Additionally, the previous researches made by our research team [21, 47] also show that types of the Zhuhai Formation sandstones are basically the same in different locations and the consistent original depositional conditions allow no interference in the comparative study of diagenesis. The consistent sedimentary conditions of the sandstones provide a good basis for accurately comparing the differences in compaction strength with different geothermal mechanisms.

The strength of compaction can be reflected by grain contact patterns in sandstones. In the LGR, contact between detrital minerals is mainly concavo-convex (Figures 4(a) and 4(b)). In the MGR, contact between detrital minerals is mainly linear and concavo-convex (Figures 4(c) and 4(d)). Whereas in the HGR, the linear contact is dominated (Figures 4(e) and 4(f)).

Quantitative statistics from the sandstone thin sections under a microscope show that in the LGR, MGR, and HGR, the concavo-convex contact dominated in sandstones of the Zhuhai Formation accounts for 57.8%, 55.2%, and 52.9%, respectively. The values, on the whole, are with a slight reduction trend from the LGR to HGR, which implies that the compaction strength of samples in the LGR is a little bit stronger than that of sandstones in the MGR and HGR.

4.2. Compaction Porosity Loss. 69 sandstone samples of the Zhuhai Formation, with similarity in grain size, roundness, and sorting from 10 wells located in different geothermal gradients in the study area, were selected to calculate the porosity loss by compaction. The results show that the original porosities of the sandstones range from 37% to 40%. The porosity loss caused by compaction ranges from 29.1% to 34.2% with an average of 31.2% in the LGR, from 21.4% to 32.0% with an average of 27.3% in the MGR, and from 18.8% to 25.3% with an average of 23.1% in the HGR (Table 1). The compaction strength of samples in the LGR is a little bit stronger than that of sandstones in the MGR and HGR, which is consistent with the observation and statistics of the detrital grain contact pattern from the thin sections under a microscope.

4.3. Paleotemperature and Paleopressure. The homogenization and freezing temperatures of the 443 inclusions from the quartz overgrowths and in healed cracks of detrital quartz in sandstones of the Zhuhai Formation taken from 10 wells of the above three regions were measured. The measured homogenization temperature ranges from 56.0°C to 236.6°C. The freezing temperature ranges from -18.0°C to -0.1°C (Table 2). The trapping pressure of inclusions simulated ranges from 35.70 MPa to 40.16 MPa with an average of 38.02 MPa, and the pressure coefficient ranges from 0.90 to 2.57 with an average of 1.64 (Table 2).

In comparison the homogenization temperature and trapping pressure of inclusions with the present temperature and pressure of the Zhuhai Formation, it is found that the homogenization temperature of inclusions exceeds the maximum present temperature of the formation and that the trapping pressure of inclusions is higher than that of the present pressure. The homogenization temperature of inclusions measured in sandstones from the LGR, MGR, and HGR, which is higher than the formation temperature, accounts for 18.3%, 7.6%, and 28.7%, respectively (Figure 5(a)). In the LGR, the paleopressure coefficients simulated from wells range from 0.90 to 1.47 with an average of 1.17. In the MGR, the paleopressure coefficient simulated ranges from 1.79 to 1.96 with an average of 1.88. Whereas in the HGR, the paleopressure coefficient ranges from 1.79 to 2.57 with an average of 2.27. The simulated paleopressure is greater than the present formation pressure in the MGR and HGR (Figure 5(b)), and the paleopressure coefficients of the MGR and HGR are also obviously higher than the present pressure coefficients (Figure 5(c)).

5. Discussion

5.1. Reservoirs in the MGR and HGR Were Affected by Thermal Fluid Activities. A prolonged phase of postrift magmatism on the highly extended crust of the Baiyun Sag has been discovered, including two major stages of magmatic activities: the first episode occurred at the start of the Miocene (23.8 Ma) and the second ones occurred at the end of the Early Miocene (17.6 Ma) [48]. Magmatism in the Baiyun

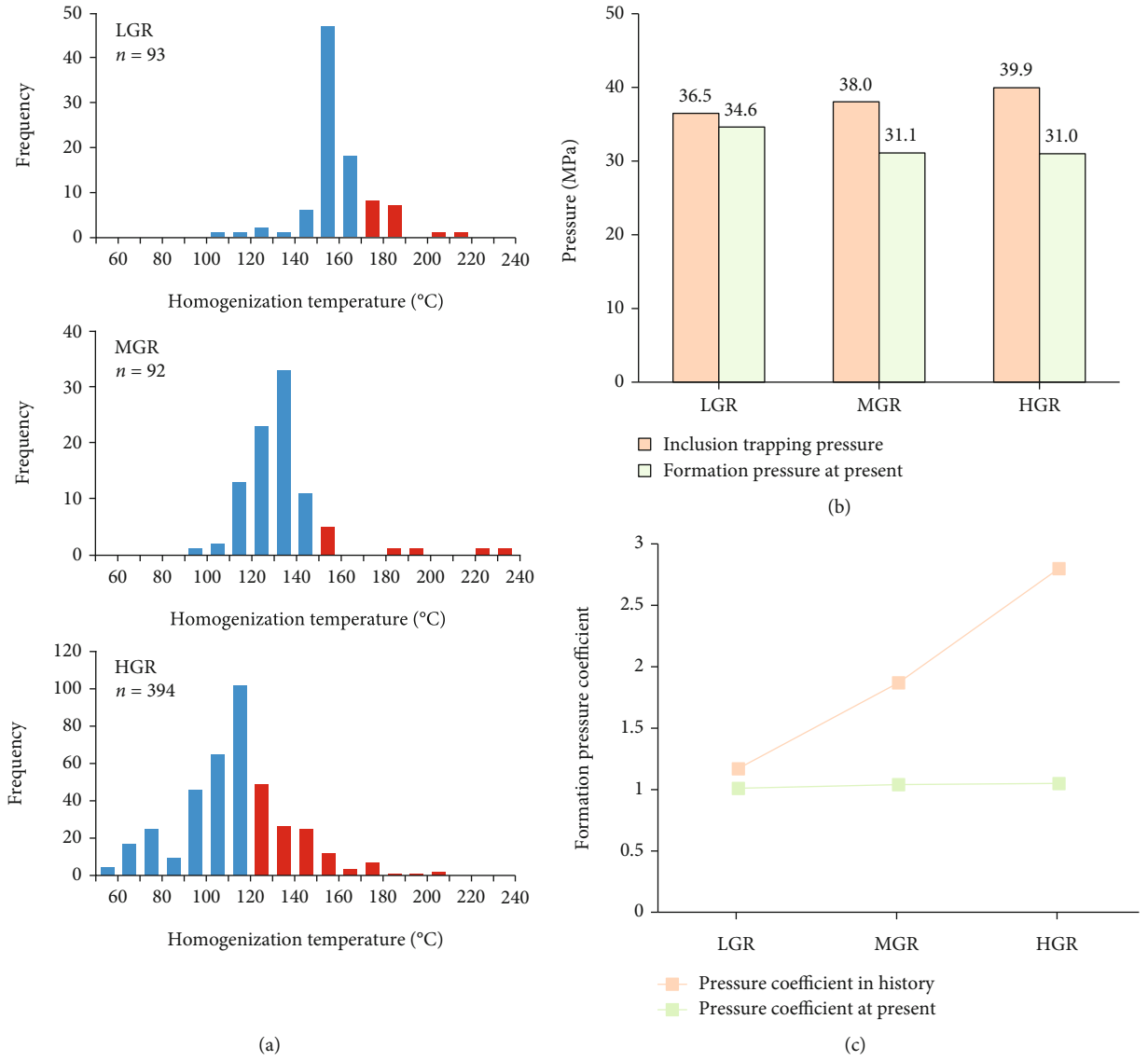

Figure 5: (a) Homogenization temperature frequency of inclusions, the red color represents the inclusions which homogenization temperature beyond the highest temperature of the Zhuhai Formation, and the blue color represents the inclusions which homogenization temperature below the highest temperature of the Zhuhai Formation. (b) Comparison of inclusion trapping pressure and formation pressure at present. (c) Comparison of paleopressure coefficient and formation pressure coefficient at present.

Sag reflects a progressive continental breakup, representing postrift tectonic thermal events associated with the continental breakup process [37]. Then, a Neotectonic movement called the Dongsha movement occurring since 13.8 Ma continuously made the faulting and thermal fluid activities more intense [48] and resulted in a number of gas chimneys and high-angle faults penetrated from the Paleogene to the Neogene strata in the Baiyun Sag, which are considered as the main migration channels for thermal fluids during the postrift stage, especially after 13.8 Ma [49–51].

Previous research on carbon, oxygen, and strontium isotopes of carbonate cements of sandstones in the Zhuhai Formation from the Baiyun Sag shows that the diagenetic fluids in the Zhuhai Formation are organic and inorganic mixed origin [45, 46]. The formation of ferrocalcite and ankerite in the Zhuhai Formation is not only related to the decarboxylation of organic acids but also closely related to the migration and accumulation of CO_2 contained inorganic thermal fluids from the deep [18, 45, 52]. During and after the Neotectonic movement, the Zhuhai Formation was invaded by thermal fluids that migrated along deep faults and gas chimneys, which caused the thermal conditions and diagenetic processes of the Paleogene strata changed [12]. As major magmatism is found in the southern Baiyun Sag [53], thermal fluid activities in the Baiyun Sag increase from north to south, which is pronounced in the MGR and HGR.

The pressure evolution of the formation in the Baiyun Sag indicates that a large-scale pressurization-relief process existed since the deposition of the Zhuhai Formation (approximately 30 Ma) [54]. From 30 Ma to 13.8 Ma, the process of the pressurization in the Baiyun Sag caused the residual pressure and pressurization rate of the Zhuhai Formation

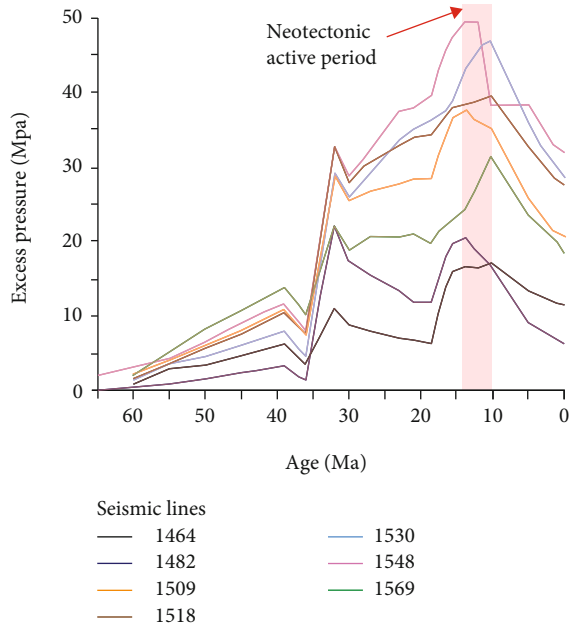

Figure 6: Formation pressure evolution in Baiyun Sag (modify from [55]).

to gradually increase, and the residual pressure reached a peak during a period approximately from 13.8 Ma to 10.5 Ma. After the Neotectonic movement, the residual pressure was rapidly released (Figure 6), and the formation pressure decreased and reached the present normal pressure in the formation.

It is confirmed that paleotemperature and paleopressure levels in the MGR and HGR were higher than those in the present formation which is proved by the inclusion homogenization temperature and simulated trapping pressure. The thermal fluid activities changed the temperature and pressure of the Zhuhai Formation and caused intensive corresponding water-rock reactions.

Additionally, typical hydrothermal origin minerals such as dawsonite, barite, and albite and anomalies of vitrinite reflectance (R_o) are found in the Zhuhai Formation and in upper strata as well from the MGR and HGR [12, 20]. Dawsonite is a tracer that provides records of CO_2 migration and geofluid transfer between deep and shallow [55]. The appearance of authigenic albite in reservoirs indicates not only the presence of sodium-rich fluids in pores but also strong water-rock reactions in formations [56]. Barite, mainly related to the mixing of high-temperature hydrothermal fluid with seawater and often enriched around seafloor hydrothermal vents [57], is an important indicator of marine hydrothermal deposition. These hydrothermal originated minerals confirm that the thermal conditions have affected the Zhuhai Formation in the MGR and HGR and the superheated fluids participated in the diagenesis. Furthermore, the distribution of R_o with depth varies in different geothermal gradient regions [12, 22]. In the LGR, the significant transition of R_o mainly occurred and the heat flow reached the peak approximately from 36.0 Ma to 30 Ma and gradually decreased after 30 Ma, which implies that the thermal conditions of the reservoirs in the LGR were mainly influenced by the Zhuqiong movement and Nanhai movement occurred in the Paleogene. However, in the MGR and HGR, the significant transition of R_o dominantly occurred at 23.8 Ma, suggesting that the reservoirs were mainly affected by the Baiyun movement and Neotectonic movement [12, 22]. Reservoirs in the MGR and HGR have been influenced by thermal fluid activities, and regions with higher geothermal gradients have experienced more intense thermal modification. From 13.8 Ma to 10.5 Ma, the temperature and pressure levels of reservoirs in the MGR and HGR reached the peak, which were higher than those of the present [54, 58], while no abnormally high temperature or high-pressure processes have been found in the LGR.

5.2. Relationship between Compaction and Cementation in Reducing Porosity. In addition to compaction, cementation is another critical diagenetic process in porosity reduction, so the porosity loss caused by both compaction and cementation should be discussed. According to the volume-cement diagram [59], the samples, which the porosity loss by compaction occupies higher percentage than that by cementation, account for 81.8%, 75.0%, and 80.0% of the total samples in the LGR, MGR, and HGR, respectively (Figure 7), while cementation resulted in the porosity loss ranging from 1.0% to 9.7% with an average of 5.7% in the LGR, from 0.1% to 16.2% with an average of 4.4% in the MGR, and from 0.3% to 26.5% with an average of 7.6% in the HGR. As a whole, compaction is the major impact that led to the porosity loss of the sandstones in different geothermal gradient regions (Figure 7).

5.3. Differences in Thermal Compaction Strength in Different Geothermal Gradient Regions. Thermal fluid activities have the important influence on the diagenetic process of the Zhuhai Formation due to high and variable heat flows and tectonic thermal events that occurred in the Baiyun Sag. Characteristics of the thermal compaction in different geothermal gradient regions may be diverse due to the different temperature and pressure evolution processes of reservoirs. Reservoirs in the Zhuhai Formation are controlled not only by the static compaction effect caused by the load of overlying formations but also by the thermal compaction effect caused by high temperature setting and thermal fluid activities.

Although there are few differences in the overall compaction effects on sandstones in different geothermal gradient regions (Table 1), the rate of porosity and permeability decrease with increasing burial depth displays as the same as a general pattern. The statistics based on the Zhuhai Formation sandstones show that the maximum porosity of the reservoir in LGR decreases from 36.0% to 10.2% at a rate of 1.0%/100 m within depth of 2,501 m (from 1,463 m to 3,964 m). The maximum porosity of the reservoir in MGR reduces from 34.7% to 10.9% at a rate of 1.7%/100 m within depth of 1,441 m (from 1,651 m to 3,092 m), and in HGR the maximum porosity of the reservoir decreases from 36.1% to 8.0% at a rate of 1.4%/100 m in depth of 1,972 m

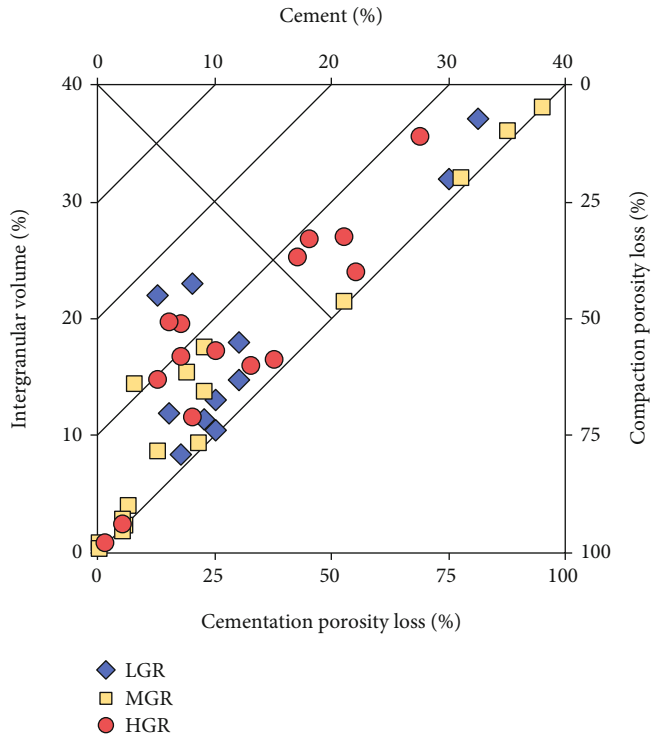

Figure 7: The intergranular volume-cement diagram for evaluation of relative importance of compaction and cementation to porosity loss of sandstone samples in different geothermal gradient regions.

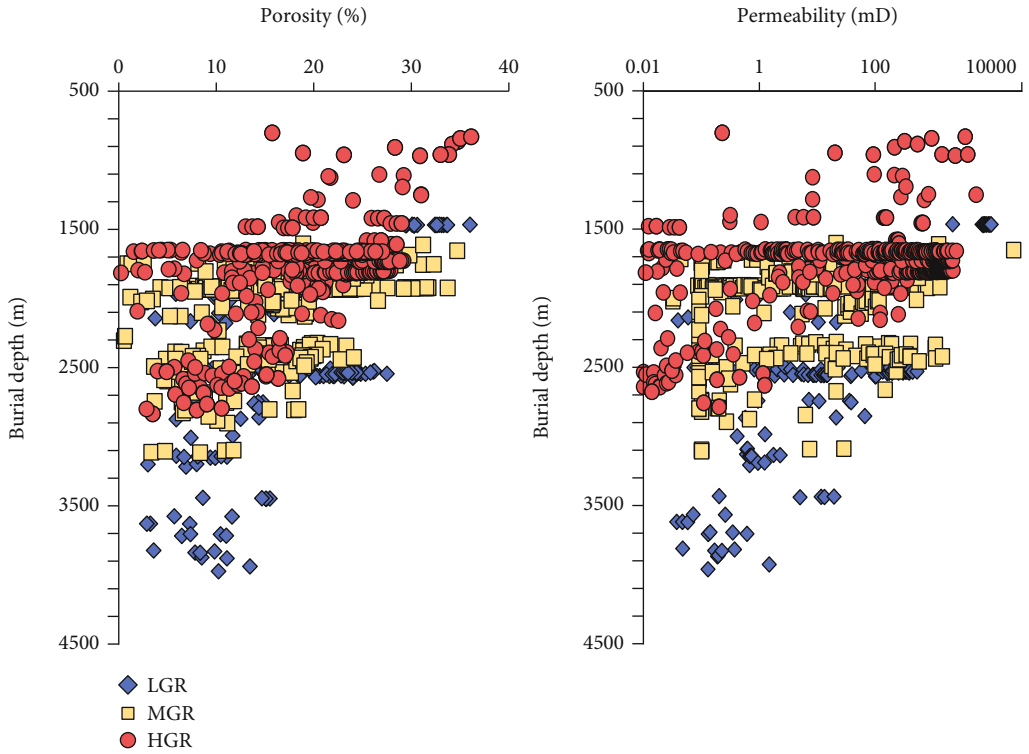

Figure 8: The variation of porosity and permeability versus burial depth of samples in different geothermal gradient regions (modified from [21]).

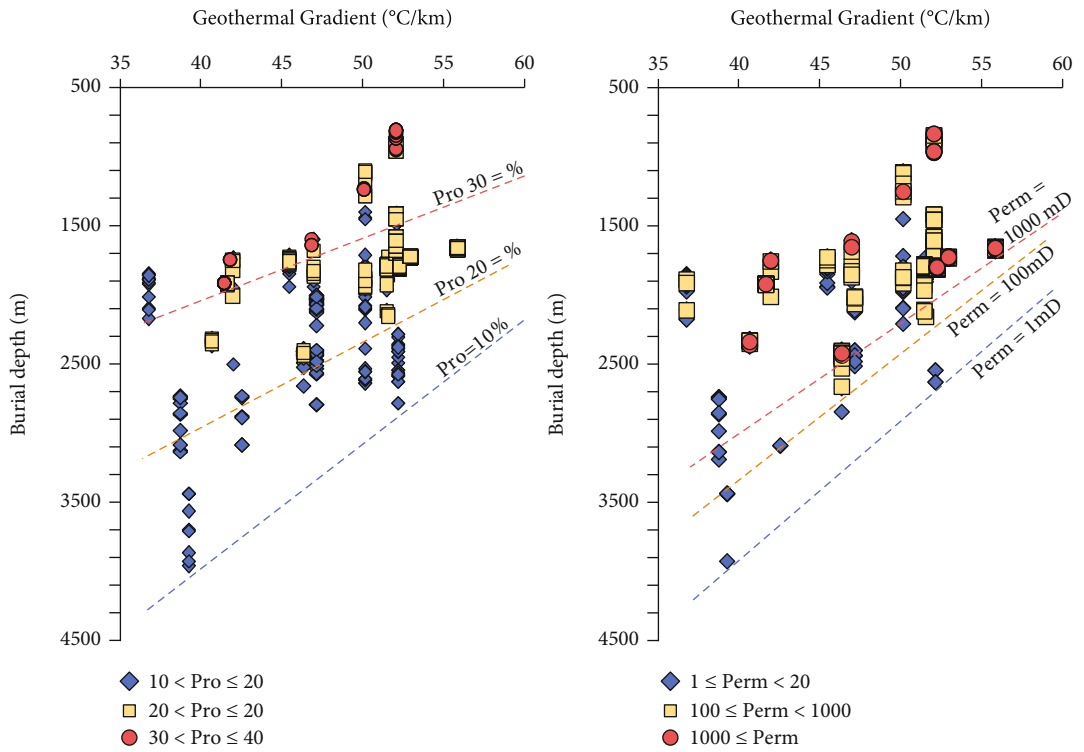

Figure 9: The variation of the limit burial depths of samples with the same porosity and permeability in different geothermal gradient regions (modified from [22]).

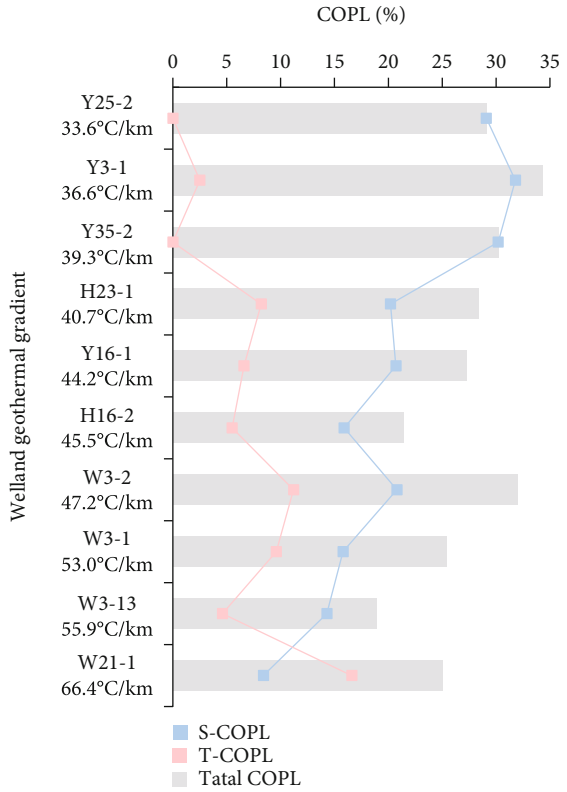

Figure 10: The characteristics of S-COPL and T-COPL in different geothermal gradient regions.

(from 828 m to 2,800 m) (Figure 8). The relationship between permeability and buried depth also displays the same trend (Figure 8).

Additionally, the burial depth of samples with nearly the same porosity and permeability is significantly shallower with an increase in geothermal gradient, and porosity and permeability decrease rapidly with an increase in burial depth in the area with a higher geothermal gradient. For example, when the geothermal gradient increases from 35°C/km to 55°C/km, the lowest buried limit of sandstone samples with 10%, 20%, and 30% porosity decreases from approximately 4,400 m, 3,200 m, and 2,200 m to approximately 2,700 m, 1,800 m, and 1,300 m, respectively, and the lowest buried limit of samples with 1 mD, 100 mD, and 1000 mD permeability dropped from approximately 4,300 m, 3,700 m, and 3,300 m to approximately 2,500 m, 2,000 m, and 1,800 m, respectively (Figure 9). The above facts indicate that the compaction rate of sandstones increases significantly with an increasing heating rate. The higher the geothermal gradient is, the more obvious and intense the thermal compaction effect is [10, 13].

To intuitively understand the impact of thermal fluid activities on the compaction process, porosity loss caused by the static compaction effect and thermal compaction effect is distinguished based on the calculation of compaction porosity loss.

From wells available in the study area, the Y25-2 well with the lowest geothermal gradient (Gra = 33.6°C/km) is selected as the reference well, and it is assumed that the calculated compaction porosity loss of sandstones in this well

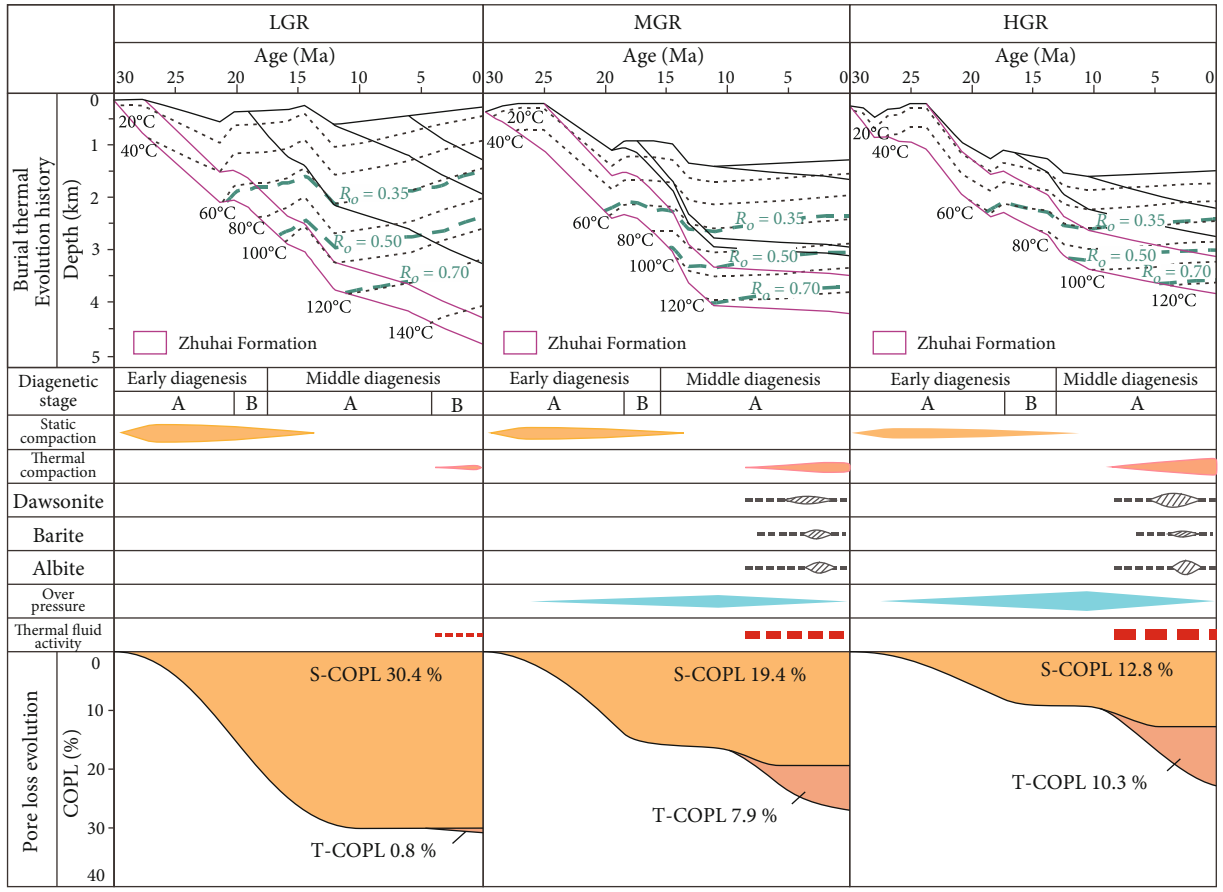

Figure 11: Burial-diagenetic-COPL model in different geothermal gradient regions.

is caused entirely by the static compaction effect, and the relative static compaction rate σ (σ equals the porosity loss in static compaction due to the overburden load at the buried depth) calculated from well Y25-2 is 8.6% per kilometer. The static compaction porosity loss (S-COPL) of the remaining wells in the study area can be calculated with σ, and the thermal compaction porosity loss (T-COPL) can be obtained as the COPL minus the S-COPL.

The burial depth of the Zhuhai Formation in each region varies greatly. On the whole, it gradually becomes shallower from the LGR (north of the Baiyun Sag) to the HGR (south of the Baiyun Sag). The upper burial depth of the Zhuhai Formation in well Y25-2 (Gra = 33.6°C/km) is approximately 3,374.1 m, and it is approximately 972.3 m in well W21-1 (Gra = 66.4°C/km). The differentiation in static compaction strength in each region is attributed to variation in burial depths of the Zhuhai Formation, and it is in turn led to a decreasing trend in S-COPL from the LGR to the HGR (Figure 10).

However, differences in the total compaction effect and porosity loss of wells in each region are unobvious. Selected sandstone samples in this study are considered adequate because the lithology, grain size, roundness, sorting characteristics, and matrix content of sandstones in each region are almost the same. The differences in sandstone porosity loss in each geothermal gradient region are considered not affected by the original sedimentary conditions but mainly by thermal conditions, due to the consistency of original sedimentary conditions.

Research shows that in the LGR, the compaction of sandstone reservoirs is dominated by the static compaction effect, the S-COPL and the T-COPL on average are 30.4% and 0.8%, respectively, and sandstone reservoirs are largely unaffected by thermal fluid activities. In the MGR, the S-COPL and the T-COPL on average are 19.4% and 7.9% on average, respectively, and in the HGR, the S-COPL and the T-COPL on average is 12.8% and 10.3%, respectively. The high proportion of T-COPL found in the MGR and HGR indicates that the compaction of the Zhuhai Formation sandstones in these two regions is obviously affected by thermal setting and fluid activities.

5.4. Differential Compaction Process and Its Relationship to Thermal Fluid Activities. The sandstone reservoirs of the Zhuhai Formation in the LGR have not suffered large-scale uplift processes and nearly have not been affected by thermal fluid activities, so the temperature of the Zhuhai Formation increases slowly with increasing burial depth, and the current formation temperature represents the highest formation temperature reached during the diagenetic process [21]. The paleopressure of the Zhuhai Formation in the LGR recovered by inclusion trapping pressure is almost the same as the present formation pressure, showing no overpressure in the Zhuhai Formation in the LGR during the diagenetic

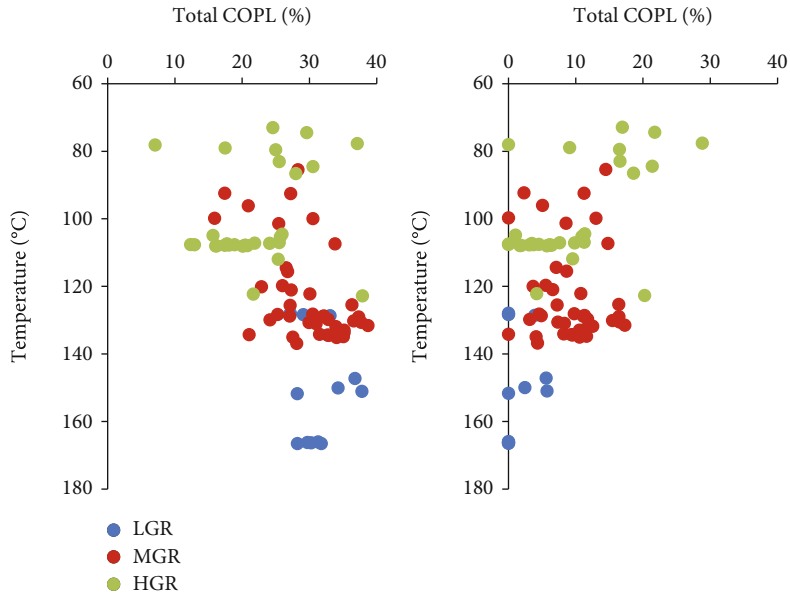

Figure 12: The total COPL and T-COPL vary with the present formation temperature in different geothermal gradient regions.

process. Under the stable temperature and pressure conditions, the compaction mode of sandstone reservoirs in the LGR is dominated by static compaction that occurred mainly at the eodiagenetic stage (from 30 Ma to 17.5 Ma), gradually weakened at the mesodiagenetic stage, and completely stopped at approximately 10 Ma. In the late mesodiagenetic stage (from approximately 5 Ma to now), there was little T-COPL in sandstone reservoirs in the LGR due to the deep burial depth and high formation temperature of the Zhuhai Formation in the LGR (Figure 11).

In the MGR and HGR, the overpressure and temperature of formations gradually increased from approximately 30 Ma to 13.8 Ma. After the Neotectonic movement (approximately 13.8 Ma), the overpressure rapidly leaked, and after that, the formation temperature was higher than that of the present due to the thermal fluid activities. In the eodiagenetic stage and early mesodiagenetic stage (from 30 Ma to 13.8 Ma), the compaction mode of sandstone reservoirs in the MGR and HGR was dominated by static compaction, and due to overpressure in the Zhuhai Formation, static compaction declined (Figure 11). In the late mesodiagenetic stage (from 13.8 Ma to now), overpressure leaking created the overlying formation loading pressure became greater than the porosity pressure, and the static compaction process was reactivated. In addition, intense thermal fluid activities occurred after the overpressure release, and thermal compaction intensified the compaction (Figure 11). There are little differences in the maximum compaction strength exerted on the Zhuhai Formation among these three regions, due to thermal compaction that occurred in the MGR and HGR, although static compaction in the MGR and HGR is relatively weak (Figure 12). The T-COPL value of sandstones in the MGR and HGR is higher than that of in the LGR, although the present formation temperature in the MGR and HGR is lower than that in the LGR (Figure 12).

6. Conclusion

Thermal setting and thermal fluid activities can affect the compaction of sandstone reservoirs. Characteristics of the thermal compaction in different geothermal gradient regions are diverse due to the different temperature and pressure evolution processes of reservoirs. The porosity loss of the Zhuhai Formation in the MGR and HGR is affected not only by the static compaction effect but also by the thermal compaction effect attributed to the abnormal high temperature and pressure conditions. And the compaction rate of sandstones increases significantly with an increasing heating rate. The higher the geothermal gradient is, the more obvious and intense the thermal compaction effect is.

Both the static and thermal compaction attributed to the porosity loss in the MGR and HGR, and the static compaction is relatively less significant than the thermal compaction and than that of in the LGR. The porosity loss caused by the thermal compaction ranges from 5.5% to 11.2% with an average of 7.9% and from 4.6% to 16.6% with an average of 10.2% in the MGR and HGR, respectively. The porosity loss caused by the static compaction ranges from 15.9% to 20.8% with an average of 19.4% and from 8.4% to 15.8% with an average of 12.8% in the MGR and HGR, respectively.

The compaction in the MGR and HGR began to restart, due to overpressure leakage and thermal fluid activities during the late mesodiagenetic stage. Overpressure release created the overlying formation loading pressure became greater than the porosity pressure, and the static compaction process was reactivated. In addition, intense thermal fluid activities occurred after the overpressure release, and thermal compaction intensified the compaction; thus, the total compaction strength of sandstones in the MGR and HGR exceeds the strength generated only by S-COPL.

Data Availability

The data used to support the findings of this study are available from the corresponding author upon request.

Conflicts of Interest

The authors declare no conflict of interest.

Acknowledgments

This study was financially supported by the National Natural Science Foundation of China: diagenetic response and fluid activity in high thermal and overpressure setting and their impact on reservoir diagenetic-pore evolution (No. 41972129), and the National Science and Technology Key Project of China: diagenetic evolution and fluid flow characteristics in the carrier layer architecture of the clastic rocks (No. 2017ZX05008-004-004-001).

References

[1] U. K. Benjamin and J. I. Nwachukwu, "Model compaction equation for hydrostatic sandstones of the Niger Delta," *IFE Journal of Science*, vol. 1, pp. 161–174, 2011.

[2] J. Lai, G. Wang, S. Wang et al., "Review of diagenetic facies in tight sandstones: diagenesis, diagenetic minerals, and prediction via well logs," *Earth-Science Reviews*, vol. 185, pp. 234–258, 2018.

[3] M. Li, R. Zhu, Z. Lou et al., "Diagenesis and its impact on the reservoir quality of the fourth member of Xujiahe Formation, Western Sichuan Depression, China," *Marine and Petroleum Geology*, vol. 103, pp. 485–498, 2019.

[4] S. E. Okunuwadje, S. A. Bowden, and D. I. M. Macdonald, "Diagenesis and reservoir quality in high-resolution sandstone sequences: an example from the Middle Jurassic Ravenscar sandstones, Yorkshire CoastUK," *Marine and Petroleum Geology*, vol. 118, p. 104426, 2020.

[5] S. Varkouhi, J. A. Cartwright, and N. J. Tosca, "Anomalous compaction due to silica diagenesis – textural and mineralogical evidence from hemipelagic deep-sea sediments of the Japan Sea," *Marine Geology*, vol. 426, article 106204, 2020.

[6] F. H. Nader, F. Champenois, M. Barbier et al., "Diagenetic effects of compaction on reservoir properties: the case of early callovian "Dalle Nacree" formation (Paris basin, France)," *Journal of Geodynamics*, vol. 101, pp. 5–29, 2016.

[7] V. H. Nguyen, N. Gland, J. Dautriat, C. David, J. Wassermann, and J. Guélard, "Compaction, permeability evolution and stress path effects in unconsolidated sand and weakly consolidated sandstone," *International Journal of Rock Mechanics and Mining Sciences*, vol. 67, pp. 226–239, 2014.

[8] M. J. Heap, N. Brantut, P. Baud, and P. G. Meredith, "Time-dependent compaction band formation in sandstone," *Journal of Geophysical Research: Solid Earth*, vol. 120, no. 7, pp. 4808–4830, 2015.

[9] A. Brüch, S. Maghous, F. L. B. Ribeiro, and L. Dormieux, "A constitutive model for mechanical and chemo-mechanical compaction in sedimentary basins and finite element analysis," *International Journal for Numerical and Analytical Methods in Geomechanics*, vol. 40, no. 16, pp. 2238–2270, 2016.

[10] S. Jianfeng, Z. Huiliang, S. Yang, W. Xi, Z. Guohua, and S. Chunsong, "Diagenetic mechanisms of sandstone reservoirs in China oil and gas-bearing basins," *Acta Petrologica Sinica*, vol. 22, no. 8, pp. 2165–2170, 2006.

[11] G. D. Jones and Y. Xiao, "Geothermal convection in South Atlantic subsalt lacustrine carbonates: developing diagenesis and reservoir quality predictive concepts with reactive transport models," *AAPG Bulletin*, vol. 97, no. 8, pp. 1249–1271, 2013.

[12] C. Li, J. Luo, H. Hu et al., "Thermal dynamic impact on deep-water sandstone diagenetic evolution of Zhuhai Formation in Baiyun Sag, Pearl River Mouth Basin," *Earth Science*, vol. 44, no. 2, pp. 572–587, 2019.

[13] G. Hou, Y. Ji, H. Wu, L. Li, Y. Wang, and W. Wang, "Quantitative characterization on the influence factors of porosity and permeability characteristics of clastic reservoirs by physical experiment simulation," *Geological Science and Technology Information*, vol. 36, no. 4, pp. 153–159, 2017.

[14] K. Liu, S. C. George, X. Lu, S. Gong, H. Tian, and L. Gui, "Innovative fluorescence spectroscopic techniques for rapidly characterising oil inclusions," *Organic Geochemistry*, vol. 72, pp. 34–45, 2014.

[15] T. Mernagh, "A review of fluid inclusions in diagenetic systems," *Acta Geologica Sinica*, vol. 89, no. 3, pp. 697–714, 2015.

[16] C. Yu, R. Zhong, R. Bai, Y. Wang, and Y. Ling, "A method to predict the homogenization temperatures of easily decrepitated fluid inclusions," *Ore Geology Reviews*, vol. 117, p. 103311, 2020.

[17] X. Chang, Y. Wang, B. Shi, and Y. Xu, "Charging of carboniferous volcanic reservoirs in the eastern Chepaizi uplift, Junggar Basin (northwestern China) constrained by oil geochemistry and fluid inclusion," *AAPG Bulletin*, vol. 103, no. 7, pp. 1625–1652, 2019.

[18] H. Ping, H. Chen, P. Zhai, J. Zhu, and S. C. George, "Petroleum charge history in the Baiyun depression and Panyu lower uplift in the Pearl River Mouth Basin, northern South China Sea: constraints from integration of organic geochemical and fluid inclusion data," *AAPG Bulletin*, vol. 103, no. 6, pp. 1401–1442, 2019.

[19] V. B. Polyakov, E. G. Osadchii, M. V. Voronin et al., "Iron and sulfur isotope factors of pyrite: data from experimental Mössbauer spectroscopy and heat capacity," *Geochemistry International*, vol. 57, no. 4, pp. 369–383, 2019.

[20] J. N. Cammack, M. J. Spicuzza, A. J. Cavosie et al., "SIMS microanalysis of the Strelley Pool Formation cherts and the implications for the secular-temporal oxygen-isotope trend of cherts," *Precambrian Research*, vol. 304, pp. 125–139, 2018.

[21] C. Lei, J. Luo, X. Pang, C. Li, J. Pang, and Y. Ma, "Impact of temperature and geothermal gradient on sandstone reservoir quality: the Baiyun Sag in the Pearl River Mouth Basin study case (northern South China Sea)," *Minerals*, vol. 8, no. 10, p. 452, 2018.

[22] J. L. Luo, M. He, X. Pang et al., "Diagenetic response on thermal evolution events and high geothermal gradients in the southern Pearl River Mouth Basin and its enlightenment to hydrocarbon exploration," *Acta Petrolei Sinica*, vol. 40, no. A1, pp. 90–104, 2019.

[23] G. C. Zhang, H. Z. Yang, Y. Chen et al., "The Baiyun Sag: a giant rich gas-generation sag in the deepwater area of the Pearl River Mouth Basin," *Natural Gas Industry*, vol. 34, no. 11, pp. 11–25, 2014.

[24] W. T. Chen, J. Y. Du, G. S. Long, S. Zhang, and X. Li, "Analysis on controlling factors of marine sequence statigraphy evolution in PearlRiver Mouth Basin," *Acta Sedimentologica Sinica*, vol. 30, no. 1, pp. 73–83, 2012.

[25] C. K. Morley, "Major unconformities/termination of extension events and associated surfaces in the South China Seas: review and implications for tectonic development," *Journal of Asian Earth Sciences*, vol. 120, pp. 62–86, 2016.

[26] X. Shi, E. Burov, S. Leroy, X. Qiu, and B. Xia, "Intrusion and its implication for subsidence: a case from the Baiyun Sag, on the northern margin of the South China Sea," *Tectonophysics*, vol. 407, no. 1-2, pp. 117–134, 2005.

[27] X. Pang, C. M. Chen, L. Shao et al., "Baiyun movement, a great tectonic event on the Oligocene-Miocene boundary in the northern South China Sea and its implications," *Geological Review*, vol. 53, no. 2, pp. 145–151, 2007.

[28] J. F. Wu, G. C. Zhang, P. J. Wang, X. J. Xie, S. B. Hu, and J. F. Qi, "Geological response and forming mechanisms of 23.8 Ma tectonic events in deepwater area of the Pearl River Mouth Basin in South China Sea," *Earth Science*, vol. 37, no. 4, pp. 654–666, 2012.

[29] Y. F. Zhang, Z. Sun, and X. Pang, "The relationship between extension of lower crust and displacement of the shelf break," *Earth Sciences*, vol. 44, no. 3, pp. 488–496, 2014.

[30] Q. Ye, L. Mei, H. Shi, Y. Shu, G. Camanni, and J. Wu, "A low-angle normal fault and basement structures within the Enping Sag, Pearl River Mouth Basin: insights into late Mesozoic to early Cenozoic tectonic evolution of the South China Sea area," *Tectonophysics*, vol. 731-732, pp. 1–16, 2018.

[31] Z. Zhou, L. Mei, J. Liu, J. Zheng, L. Chen, and S. Hao, "Continentward-dipping detachment fault system and asymmetric rift structure of the Baiyun Sag, northern South China Sea," *Tectonophysics*, vol. 726, no. 1, pp. 121–136, 2018.

[32] T. Xiao-Yin, H. Sheng-Biao, Z. Gong-Cheng et al., "Characteristic of surface heat flow in the Pearl River Mouth Basin and its relationship with thermal lithosphere thickness," *Chinese Journal of Geophysics*, vol. 57, no. 6, pp. 1857–1867, 2014.

[33] Y. Song, C. Y. Zhao, G. C. Zhang, H. B. Song, J. N. Shan, and L. Chen, "Research on tectono-thermal modeling for Qiongdongnan Basin and Pearl River Mouth Basin in the northern South China Sea," *Chinese Journal of Geophysics*, vol. 54, no. 12, pp. 3057–3069, 2011.

[34] S. S. Nissen, D. E. Hayes, Y. Bochu, W. Zeng, Y. Chen, and X. Nu, "Gravity, heat flow, and seismic constraints on the processes of crustal extension: northern margin of the South China Sea," *Journal of Geophysical research: Solid Earth*, vol. 100, no. B11, pp. 22447–22483, 1995.

[35] X. Shi, X. Qiu, K. Xia, and D. Zhou, "Characteristics of surface heat flow in the South China Sea," *Journal of Asian Earth Sciences*, vol. 22, no. 3, pp. 265–277, 2003.

[36] L. J. Mi, Y. S. Yuan, G. C. Zhang, S. B. Hu, L. J. He, and S. C. Yang, "Characteristics and genesis of geothermal field in deep-water area of the northern South China Sea," *Acta Petrolei Sinica*, vol. 30, no. 1, pp. 27–32, 2009.

[37] Y. Yuan, W. Zhu, L. Mi, G. Zhang, S. Hu, and L. He, ""Uniform geothermal gradient" and heat flow in the Qiongdongnan and Pearl River Mouth Basins of the South China Sea," *Marine and Petroleum Geology*, vol. 26, no. 7, pp. 1152–1162, 2009.

[38] D. C. Beard and P. K. Weyl, "Influence of texture on porosity and permeability of unconsolidated sand," *AAPG Bulletin*, vol. 57, no. 2, pp. 349–369, 1973.

[39] S. N. Ehrenberg, "Assessing the relative importance of compaction processes and cementation to reduction of porosity in sandstones: discussion; compaction and porosity evolution of Pliocene sandstones, Ventura Basin, California: discussion," *The American Association of Petroleum Geologists Bulletin*, vol. 73, no. 10, pp. 1274–1276, 1989.

[40] D. L. Hall, S. M. Sterner, and R. J. Bodnar, "Freezing point depression of NaCl-KCl-H 2 O solutions," *Economic Geology*, vol. 83, no. 1, pp. 197–202, 1988.

[41] Y. G. Zhang and J. D. Frantz, "Determination of the homogenization temperatures and densities of supercritical fluids in the system $NaClKClCaCl_2H_2O$ using synthetic fluid inclusions," *Chemical Geology*, vol. 64, no. 3-4, pp. 335–350, 1987.

[42] X. Wang, Y. L. Jiang, L. Z. Cao, H. Liu, and W. J. Zhang, "Charateristics of paleopressure evolution and its influencing factors in sub-sags of hydrocarbon-bearing sag: a case study of Raoyang sag in Jizhong depression," *Journal of China University of Mining and Technology*, vol. 46, no. 3, pp. 586–595, 2017.

[43] B. Liu and K. Shen, *Thermal Mechanics of Fluid Inclusions*, Geology Press, Beijing, China, 1999.

[44] J. F. Shou and G. H. Zhu, "Study on quantitative prediction of porosity preservation in sandstone reservoirs," *Scientia Geologica Sinica*, vol. 33, no. 2, pp. 118–124, 1998.

[45] D. F. Wang, J. L. Luo, S. H. Chen, H. U. Haiyan, M. A. Yongkun, and L. I. Chi, "Carbonate cementation and origin analysis of deep sandstone reservoirs in the Baiyun Sag, Pearl River Mouth Basin," *Acta Geologica Sinica*, vol. 91, no. 9, pp. 2079–2090, 2017.

[46] J. Pang, J. L. Luo, Y. K. Ma et al., "Forming mechanism of ankerite in tertiary reservoir of the Baiyun Sag, Pearl River-Mouth Basin, and its relationship to CO_2-bearing fluid activity," *Acta Geologica Sinica*, vol. 93, no. 3, pp. 724–737, 2019.

[47] C. Lei, *Influence of High Thermal Background on Deep Water Reservoir Quality in the Baiyun Sag, Pearl River Mouth Basin*, Northwest University, 2019.

[48] F. Zhao, T. M. Alves, S. Wu et al., "Prolonged post-rift magmatism on highly extended crust of divergent continental margins (Baiyun Sag, South China Sea)," *Earth & Planetary Science Letters*, vol. 445, pp. 79–91, 2016.

[49] X. W. Guo, K. Y. Liu, S. He, Z. Yang, and T. T. Dong, "Quantitative estimation of overpressure caused by gas generation and application to the Baiyun depression in the Pearl River Mouth Basin, South China Sea," *Geofluids*, vol. 16, no. 1, p. 148, 2016.

[50] Q. Sun, S. Wu, J. Cartwright, and D. Dong, "Shallow gas and focused fluid flow systems in the Pearl River Mouth Basin, northern South China Sea," *Marine Geology*, vol. 315-318, pp. 1–14, 2012.

[51] Z. Sun, Z. Xu, L. Sun et al., "The mechanism of post-rift fault activities in Baiyun Sag, Pearl River Mouth Basin," *Journal of Asian Earth Sciences*, vol. 89, pp. 76–87, 2014.

[52] C. Lei, J. L. Luo, Y. K. Ma et al., "Distribution of carbon dioxide in Baiyun Sag and its periphery, Pearl River Mouth Basin," *Journal of Mineralogy and Petrology*, vol. 37, no. 3, pp. 97–106, 2017.

[53] J. Gao, S. Wu, K. McIntosh, L. Mi, Z. Liu, and G. Spence, "Crustal structure and extension mode in the northwestern margin of the South China Sea," *Geochemistry, Geophysics, Geosystems*, vol. 17, no. 6, pp. 2143–2167, 2016.

[54] H. Chen, C. Chen, X. Pang, J. Wang, and W. Shi, "Natural gas sources, migration and accumulation in the shallow water area

of the Panyu lower uplift: an insight into the deep water prospects of the Pearl River Mouth Basin, South China Sea," *Journal of Geochemical Exploration*, vol. 89, no. 1-3, pp. 47–52, 2006.

[55] F. Li, W. Li, Z. Yu, N. Liu, H. Yang, and L. Liu, "Dawsonite occurrences related to the age and origin of CO_2 influx in sandstone reservoirs: a case study in the Songliao Basin, NE China," *Geochemistry, Geophysics, Geosystems*, vol. 18, no. 1, pp. 346–368, 2017.

[56] S. Li, J. Tian, X. Lin, Y. Zuo, H. Kang, and D. Yang, "Effect of alkaline diagenesis on sandstone reservoir quality: insights from the Lower Cretaceous Erlian Basin, China," *Energy Exploration & Exploitation*, vol. 38, no. 2, pp. 434–453, 2020.

[57] E. M. Griffith, A. Paytan, U. G. Wortmann, A. Eisenhauer, and H. D. Scher, "Combining metal and nonmetal isotopic measurements in barite to identify mode of formation," *Chemical Geology*, vol. 500, pp. 148–158, 2018.

[58] L. Kong, H. Chen, H. Ping, P. Zhai, Y. Liu, and J. Zhu, "Formation pressure modeling in the Baiyun Sag, northern South China Sea: implications for petroleum exploration in deep-water areas," *Marine and Petroleum Geology*, vol. 97, pp. 154–168, 2018.

[59] D. W. Houseknecht, "Assessing the relative importance of compaction processes and cementation to reduction of porosity in sandstones," *AAPG Bulletin*, vol. 71, no. 6, pp. 633–642, 1987.